Field-induced structural control of CO_X molecules adsorbed on graphene

Manaho Matsubara, and Susumu Okada

Citation: Journal of Applied Physics **123**, 174302 (2018); doi: 10.1063/1.5029510
View online: https://doi.org/10.1063/1.5029510
View Table of Contents: http://aip.scitation.org/toc/jap/123/17
Published by the American Institute of Physics

Field-induced structural control of CO_x molecules adsorbed on graphene

Manaho Matsubara[a] and Susumu Okada[b]
Graduate School of Pure and Applied Sciences, University of Tsukuba, 1-1-1 Tennoudai, Tsukuba, Ibaraki 305-8571, Japan

(Received 15 March 2018; accepted 15 April 2018; published online 1 May 2018)

Using the density functional theory combined with both the van der Waals correction and the effective screening medium method, we investigate the energetics and electronic structures of CO and CO_2 molecules adsorbed on graphene surfaces in the field-effect-transistor structure with respect to the external electric field by the excess electrons/holes. The binding energies of CO and CO_2 molecules to graphene monotonically increase with increasing hole and electron concentrations. The increase occurs regardless of the molecular conformations to graphene and the counter electrode, indicating that the carrier injection substantially enhances the molecular adsorption on graphene. Injected carriers also modulate the stable molecular conformation, which is metastable in the absence of an electric field. *Published by AIP Publishing.*
https://doi.org/10.1063/1.5029510

I. INTRODUCTION

Because of its unique structural and electronic properties, graphene is a potential material for integration into functional devices. A two-dimensional honeycomb network of sp^2 C atoms endows graphene with pairs of linear dispersion bands at the Fermi level and six corners of the Brillouin zone, leading to a zero-gap semiconducting electronic structure.[1–3] With this peculiar electronic structure around the Fermi level, graphene exhibits remarkable carrier mobility[4–6] of up to 200 000 $cm^2 V^{-1} s^{-1}$ that enables high-speed switching within electronic devices.[7] Nevertheless, the electronic structure of graphene is fragile against the formation of hybrid structures with foreign materials, such as insulating substrates,[8–11] metal electrodes,[12] molecular/atomic adsorbates,[13–21] and structural defects.[22–26] Furthermore, an external electric field can tune the electronic structure of graphene and its hybrids.[27] That is, foreign materials can be detected by monitoring the electronic structure of graphene.[28] In our previous works, metal nanoparticles adsorbed on graphene with a field-effect transistor (FET) structure affect the carrier injection in graphene: Depending on their mutual arrangement with respect to the electrode, the nanoparticles pin the Fermi level at the energy level associated with them.

Despite the electronic structure of graphene hybrids having been well studied to date, little is known about the structural properties of graphene hybrids under external perturbations, such as the external electric field and mechanical deformations. Such studies may advance the application of graphene in sensing devices because adsorption phenomena are influenced by charge density distributions on graphene and adsorbates. Indeed, mechanical strain has been reported to cause both increases and decreases in the interaction between graphene and adsorbed C_{60}.[29] Furthermore, optimum adsorbed structures of metal nanoparticles on graphene strongly depend on the carrier density injected via the gate electrode and on their mutual arrangement with respect to the gate electrode associated with the interplay between the electron states of the metal nanoparticles and the small density of states near the Fermi level of graphene.[20] Moreover, the energetics and geometries of environmental molecules, such as CO_x and NO_x, under the external electric field are still unclear. The binding energy and the stable molecular arrangement of such molecules on graphene are expected to depend also on the carrier density and species injected under the gate voltage in FET structures. By analogy with metal nanoparticles on graphene in FET structures, this expectation would certainly further improve or tune the molecular sensing efficiency of graphene-based sensing devices.

The purpose of this work is to clarify, using density functional theory (DFT) combined with the effective screening medium (ESM) method, the energetics and the geometries of the CO and CO_2 molecules adsorbed on graphene with regard to carrier density and species injected under gate voltages for providing guiding principle to tune and control the binding properties of these molecules to graphene using an electric field. Our calculations show that the energetics and stable binding structures of CO and CO_2 adsorbed on graphene are sensitive to the carrier density and species injected by the counter gate electrode simulated by ESM. The carriers can control the binding energy and stable conformations of these molecules on graphene by tuning the carrier density and species. These results provide a guiding principle in developing graphene-based sensing and catalytic devices in terms of the external electric field.

II. CALCULATION METHOD

All calculations were performed based on DFT[30,31] using the STATE package.[32] For the calculation of the exchange-correlation energy amongst the interacting electrons, the generalized gradient approximation was used with the Perdew–Burke–Ernzerhof functional form.[33] To describe the weak dispersive interaction between CO_x molecules and graphene, we considered the van der Waals (vdW) correction

[a]Electronic mail: mmatsubra@comas.frsc.tsukuba.ac.jp
[b]Electronic mail: sokada@comas.frsc.tsukuba.ac.jp

by treating vdW-DF2 with the C09 exchange-correlation functional.[34–36] We used ultrasoft pseudopotentials generated using the Vanderbilt scheme to describe the interaction between nuclei and electrons.[37] The valence wave functions and deficit charge density were expanded in terms of the plane-wave basis set with cutoff energies of 25 and 225 Ry, respectively. Brillouin zone integration was performed with the Γ-centered $8 \times 8 \times 1$ uniform $\boldsymbol{k}$-mesh for self-consistent electronic structure calculations for graphene with a 4×4 lateral periodicity, which corresponds to a $32 \times 32 \times 1$ $\boldsymbol{k}$-mesh in a primitive 1×1 cell of graphene, resulting in sufficient convergence in the geometric and electronic structures of graphene and its derivatives. With this choice of the $\boldsymbol{k}$-mesh, the Brillouin zone integration contains the K and K′ points, enabling the phenomena associated with the Dirac point to be analyzed. Geometric structures of CO and CO_2 adsorbed on graphene were fully optimized until the remaining force acting on each atom was less than 0.005 Ry/Å without an electric field. For calculations with an electric field, the internal atomic coordinates of CO and CO_2 adsorbed on graphene are set to those without the electric field.

The ESM method was adopted to investigate the energetics and geometries of graphene adsorbing CO and CO_2 molecules under an external electric field. To inject electrons and holes into CO and CO_2 adsorbed on graphene, we considered a FET structure in which a planar counter metal electrode described by the ESM with an infinite relative permittivity is situated above the graphene at vacuum spacing of 6.35 and 9.00 Å from the center of mass of the graphene adsorbing CO and CO_2, respectively [Figs. 1(a) and 1(b)].[38] CO and CO_2 molecules are adsorbed on the electrode side of the graphene surfaces per 4×4 lateral periodicity with two representative molecular conformations characterized by their orientations (horizontal and vertical conformations) and positions (on-top and hollow sites) with regard to the graphene layer.

III. RESULTS AND DISCUSSION

Figure 2 shows the total energy of CO and CO_2 adsorbed on graphene with regard to the carrier concentration ranging from 0.3e for CO and 0.2e for CO_2 to 1.0h as a function of their spacing. The total energy, E, is calculated using

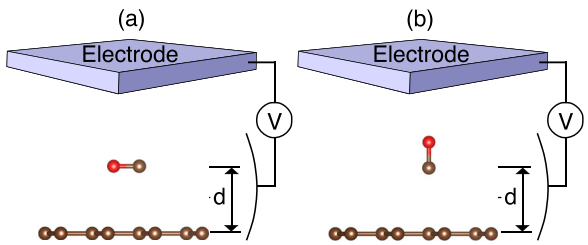

FIG. 1. Structural models of CO with (a) the lying molecular conformation and (b) the standing molecular conformation adsorbed on graphene in the FET structure. Red and brown balls denote O and C atoms, respectively. The blue slab above the molecule adsorbed on graphene represents the counter metal electrodes simulated by the ESM.

$$E = E^{F}_{\mathrm{Gra/CO_x}} - E^{0}_{\mathrm{Gra}} - E^{0}_{\mathrm{CO_x}},$$

where $E^{F}_{\mathrm{Gra/CO_x}}$, E^{0}_{Gra}, and $E^{0}_{\mathrm{CO_x}}$ are the total energies of the graphene adsorbing CO_x under an electric field, an isolated graphene without the external field, and an isolated CO_x without the external field, respectively. The energy minima without the electric field are shallow regardless of the molecular species, orientation, and mutual position, indicating that CO_x is weakly bound to graphene. The calculated binding energy of CO and CO_2 is about 0.1 eV, slightly depending on the molecular species and orientation, which is comparable to their binding energy on other two-dimensional materials.[39,40] For the lying molecular arrangement with regard to the graphene layer, the adsorption property is insensitive to the mutual position of the adsorbates, whether they are located in on-top or hollow sites of the graphene network. For a standing molecular orientation to graphene, the adsorption depends on their mutual orientation and position with respect to the hexagonal covalent network of graphene. Note that these molecules are hardly or are not bound to graphene without the vdW corrections. In contrast, by injecting carriers, energy landscapes are substantially modulated, depending on carrier species and concentrations: The energy minima are deepened and the optimum spacing decreases with increasing carrier concentration, except for the standing conformation in which the C atom is located on the electrode side. In particular, molecules in a lying conformation are tightly bound under the injection of carriers compared with conditions encountered without the electric field.

Figure 3(a) shows the optimized equilibrium spacing between the CO molecule and graphene as a function of carrier concentrations. The equilibrium spacing ranges from about 3.4 to 3.6 Å without the electric field, depending on the mutual molecular position and orientation with respect to the graphene network. For the lying molecular conformation, the optimum spacing is insensitive to the mutual position of CO on graphene. In contrast, the spacing under the standing molecular conformation is sensitive to the mutual position of the molecule on the hexagonal network of graphene. The optimum spacing for the molecule adsorbed on the hollow site is shorter than that for the on-top atomic site. Furthermore, in the standing conformation the optimum spacing between CO and graphene also depends on whether the C atom is situated on the electrode side. Among all conformations, a standing conformation at an on-top site where the C atom is not situated on the electrode side leads to the largest spacing between CO and graphene. In contrast, a standing conformation at a hollow site where the C atom is situated on the electrode side leads to the smallest spacing. Under carrier injection, the spacing monotonically decreases with increasing electron and hole concentrations, regardless of their molecular conformations. The optimum spacing is narrower by about 0.6 and 0.3 Å under the hole concentration of 1.0h and the electron concentration of 0.3e, respectively. Furthermore, the spacing exhibits an unusual feature for the standing conformation in which the C atom is situated on the electrode side:

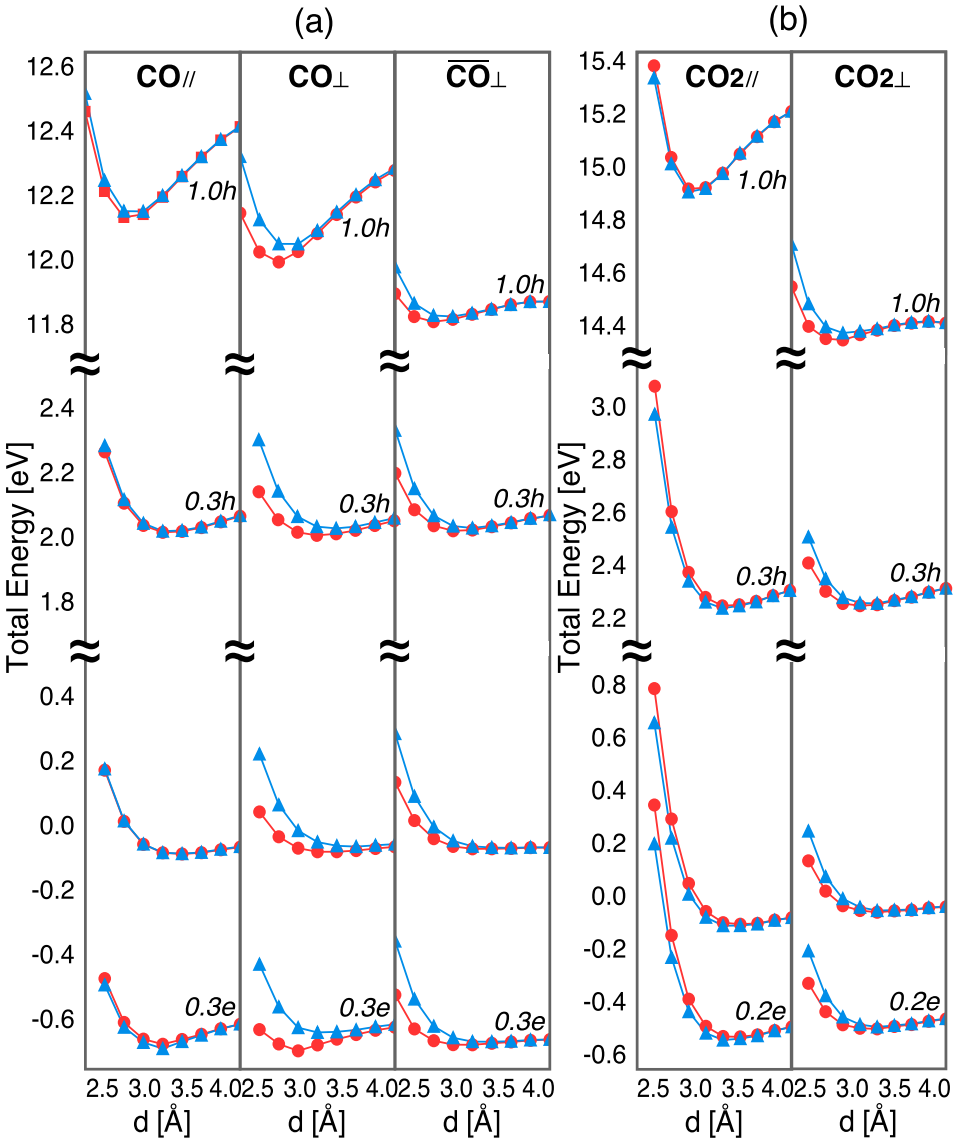

FIG. 2. Total energies of (a) CO and (b) CO_2 adsorbed on graphene as a function of the spacing between adsorbed molecules and graphene under various carrier concentrations. Circles and triangles correspond to the total energy of the C atom in the molecules adsorbed in the hollow sites and on-top sites of graphene, respectively. In each panel, the subscript symbols, ⊥ and //, indicate the standing and lying molecular conformations, respectively, to graphene. For the CO molecule, center and right panels correspond to the standing conformations in which the C atoms are situated on the graphene and electrode sides, respectively.

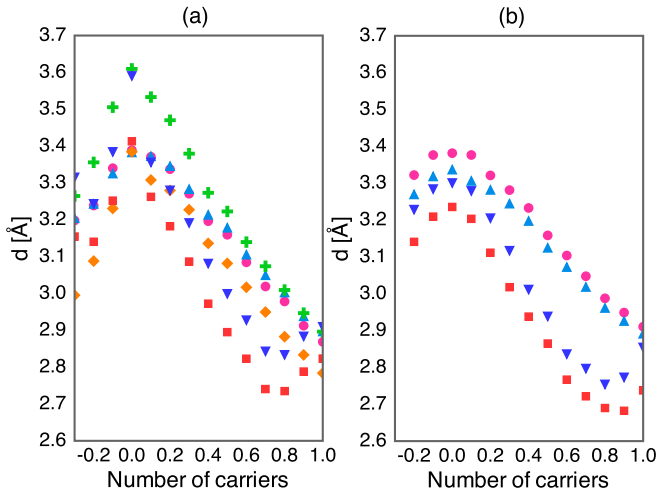

FIG. 3. Equilibrium spacing, d, between adsorbed molecules and graphene as a function of carrier concentration for (a) CO and (b) CO_2. Circles and triangles correspond to a lying molecular conformation with hollow and on-top adsorption sites, respectively. Squares and inverse triangles (rhombuses and crosses) correspond to a standing molecular conformation with hollow and on-top adsorption sites, respectively, in which for the CO molecule, the C atom is situated on the electrode side (on the graphene side).

The spacing again increases with increasing hole concentrations of 0.7h or higher and electron concentrations of 0.2e or higher.

Figure 3(b) shows the optimized equilibrium spacing between the CO_2 molecule and graphene as a function of carrier concentrations. With regard to the CO_2 molecule, the spacing is sensitive to the molecular conformation and mutual position with respect to the graphene network. The smallest spacing is about 3.2 Å under the standing conformation at the hollow site, whereas the largest spacing is about 3.4 Å under the lying conformation at the hollow site without the electric field. Furthermore, the spacing also monotonically decreases with increasing carrier concentration, regardless of their molecular arrangements, except standing conformations under hole concentrations of 0.8h or higher.

As stated above, carrier injection deepens the potential landscape of the molecule adsorbed on graphene and decreases its equilibrium spacing. This fact implies that carrier injection can control the binding properties of CO and CO_2 molecules on graphene. To give a quantitative discussion, we analyze the dynamical properties of the adsorbed molecules on graphene by calculating the frequency of

molecular oscillations around the equilibrium position on graphene under the various carrier concentrations (Fig. 4). The frequency monotonically increases with increasing numbers of electrons and holes, except for CO and CO_2 in the standing conformation and at high carrier concentration, in which the C atom is situated on the electrode side for the CO molecule. The frequencies of CO and CO_2 under a hole concentration of 0.7h are higher by about 3 and 2 times, respectively, than those under neutral conditions. Furthermore, the frequency also strongly depends on the molecular conformation for each carrier concentration. For the standing molecular conformation in which the C atom is situated on the electrode side for the CO molecule, the frequency decreases with increasing high carrier concentration; for CO adsorbed on graphene, the electron and hole concentrations are 0.2e and 0.7h or higher, respectively, and the hole concentration is 0.8h or higher in CO_2 adsorption to graphene, in accordance with the increasing equilibrium spacing. Therefore, in THz spectroscopic experiments, we can detect molecular conformations and relative positions with respect to graphene.

Figure 5 shows the relative total energy of the CO and CO_2 molecules on graphene with respect to their molecular orientation and position to graphene as a function of carrier concentration. The energies are measured from that of the lying conformation on the hollow and on-top sites for CO and CO_2, respectively, which corresponds to their ground state molecular arrangements without the electric field. Although the lying conformation is the most stable without the electric field, the injected carriers change their stable molecular orientation from lying to standing. Therefore, CO or CO_2 molecules adsorbed on graphene may undergo a structural phase transition induced by the external electric field. In that case, intermolecular interaction may also affect the molecular conformation on graphene, leading to more complex dependence of their orientation on carrier concentration.

Figure 6 shows the accumulated carrier density injected under a gate voltage for CO and CO_2 adsorbed on graphene under the equilibrium spacing as a function of the z axis

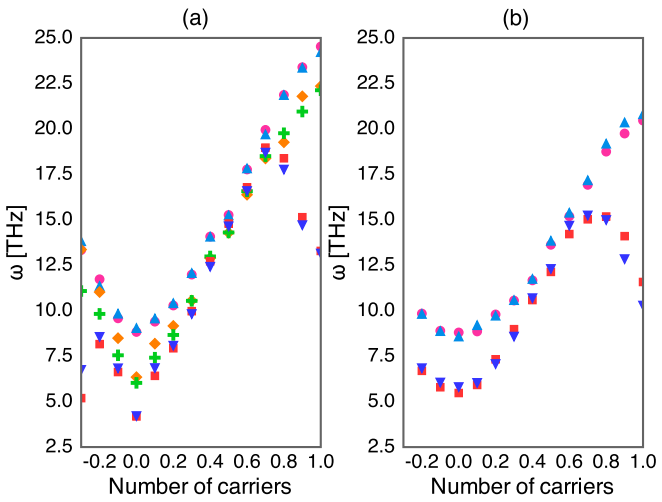

FIG. 4. Frequency of the molecular oscillation of (a) CO and (b) CO_2 molecules around the equilibrium position on graphene as a function of carrier concentration. For the meanings of the symbols, see Fig. 3.

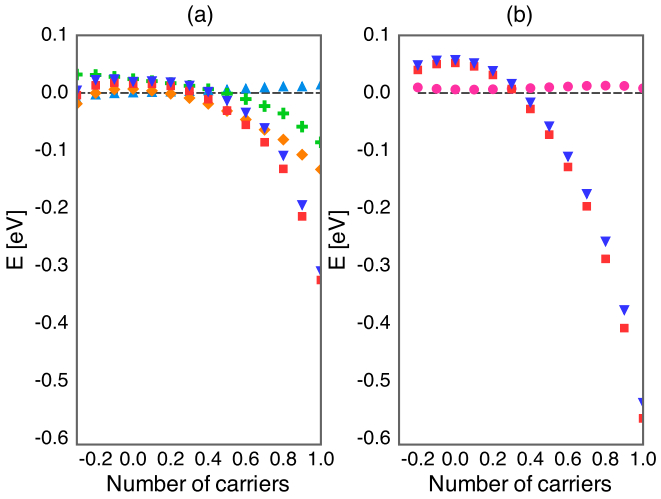

FIG. 5. Relative total energy of (a) CO and (b) CO_2 on graphene as a function of the carrier concentration. The energies are measured from that of the lying molecular arrangement on the hollow and on-top sites for CO and CO_2, respectively, which correspond to their ground state molecular arrangements without the electric field. For the meanings of the symbols, see Fig. 3.

normal to graphene. The distribution of the accumulated carrier depends on the carrier species, molecular species, and their orientation to the graphene layer. With electron doping, the electrons mainly accumulate on the electrode side of the graphene surface. Accordingly, holes and electrons are induced on the graphene and electrode sides of the CO_x molecules, respectively. Thus, the molecules possess a dipole moment with respect to the normal to the graphene surface. With hole doping, similar carrier accumulation occurs. The hole injected into the electrode side of the graphene induces electrons and holes on the graphene and electrode sides of the molecules, respectively. In this case, a similar dipole moment is induced on the adsorbed molecules by the carrier injection. The Coulomb interaction between the dipole moment induced on the molecule and the carriers on graphene may enhance the binding energy of these molecule on graphene, leading to the decrease in the equilibrium spacing and the increase in frequency under hole or electron doping. Furthermore, the distribution of the accumulated carriers on the molecule is sensitive to the molecular orientation. The distribution of the carrier density on the standing molecular conformation is wider than that on the lying one, stabilizing the standing molecular conformation under carrier injection because the Coulomb interaction between CO_x and graphene is enhanced.

Figure 7 shows the Kohn–Sham states of CO and CO_2 adsorbed on graphene near the Fermi level with respect to carrier concentration. Without the electric field, the electron states associated with the adsorbed molecules are absent near the Fermi level, indicating that the adsorbed molecules do not affect the carrier injection into the hybrid systems under low carrier concentrations. The molecular adsorption to graphene induces modulations of the energy gap between the highest occupied (HO) and the lowest unoccupied (LU) states of CO and CO_2. The gap is narrower or wider by up to 0.2 eV than that in the isolated forms, depending on molecular species and conformations. The carriers are primarily accommodated

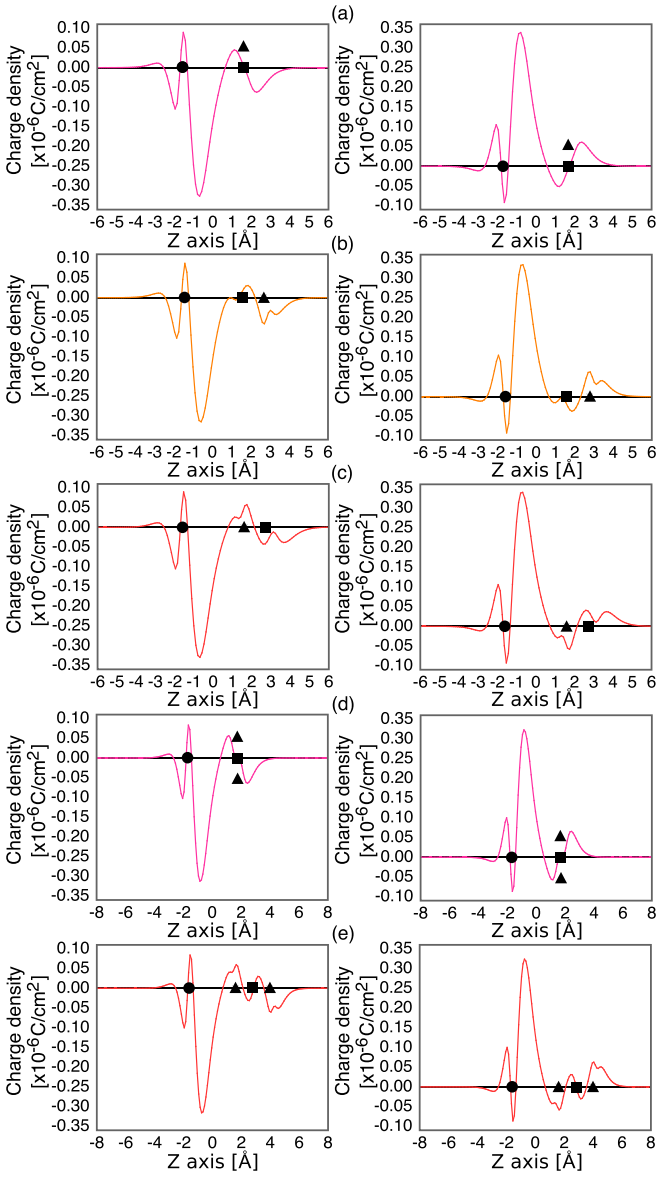

FIG. 6. Plane-integrated charge density of the injected carriers in graphene adsorbing CO with (a) the lying conformation and the standing conformations in which the C atom is located on (b) the graphene side and (c) the electrode side. Plane-integrated charge density of the injected carriers in graphene adsorbing CO_2 with (d) the lying conformation and (e) the standing conformation. In each figure, the left and right panels correspond with the charge distribution under 0.2e and 0.2h injection, respectively, by the gate voltage. Circles, squares, and triangles denote positions of the C atoms belonging to graphene, the C atoms belonging to CO_x, and the O atoms, respectively. The counter electrode is located on the right-hand side of each figure.

within the graphene sheet, leading to a monotonic shift in the Fermi level. The Dirac point retains its energy during carrier injection because of the ridged band nature of electron states of graphene upon the carrier injection. In contrast, the electron states associated with adsorbed molecules vary under carrier injection: Eigenvalues of the HO and the LU states of CO and CO_2 molecules monotonically shift downward with increasing electron concentration, whereas they shift upward with increasing hole concentration. For CO adsorption, the HO state of CO in a standing conformation in which the C atom is situated on

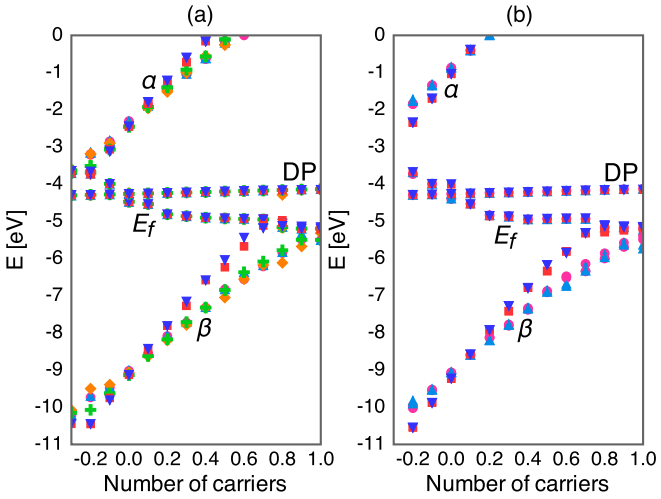

FIG. 7. Electronic structure near the Fermi level of (a) CO and (b) CO_2 adsorbed on graphene as a function of carrier concentration. DP, E_f, α, and β indicate the Dirac point of graphene, the Fermi level, the lowest unoccupied states of the adsorbed molecule, and the highest occupied states of the adsorbed molecule, respectively. For the meanings of the symbols, see Fig. 3.

the electrode side crosses the Fermi level under the hole concentration of 0.7h. The threshold carrier concentration depends on the molecular orientation. For the standing molecular conformation in which the C atom is situated on the electrode side, the threshold carrier concentration is lower than that for other molecular conformations because the distribution of the HO state in the conformation is closest to the counter electrode among the molecular conformations studied here. Above the critical carrier concentration, the eigenstates associated with CO are insensitive to the carrier injection because the Fermi level is pinned at the HO state of the CO molecule. For CO_2 adsorption, as for CO, the HO state of CO_2 in a standing conformation crosses the Fermi level at the lower hole concentration of 0.8h than that in a lying conformation. Therefore, the adsorbing properties of CO_x molecules on graphene exhibit further variation at high carrier concentrations.

IV. SUMMARY

Using DFT with the vdW correction and the ESM method, we investigated the geometries and energetics of CO and CO_2 molecules adsorbed on graphene under the external electric field. Our theoretical investigations found that the binding energies of these molecules on graphene monotonically increased with increasing carrier densities, regardless of the molecular orientation and their relative position to graphene. This fact indicates that the electric field or excess carriers control the binding properties of molecules, thereby enhancing the molecular sensing capability of graphene. Furthermore, detailed analyses regarding the geometric structure clarified that the stable molecular orientation strongly depends on the carrier concentration for both molecules: The lying conformation to graphene is the ground state under neutral conditions, whereas the standing conformation is the ground state under either electron or hole injection, whose critical density is sensitive to the direction of the C atom and the relative position of these molecules on graphene.

ACKNOWLEDGMENTS

This work was supported by JST-CREST Grant Nos. JPMJCR1532 and JPMJCR1715 from the Japan Science and Technology Agency, JSPS KAKENHI Grant Nos. JP17H01069, JP16H00898, and JP16H06331 from the Japan Society for the Promotion of Science, and the Joint Research Program on Zero-Emission Energy Research, Institute of Advanced Energy, Kyoto University. Parts of the calculations were performed on an NEC SX-Ace at the Cybermedia Center at Osaka University and on an SGI ICE XA/UV at the Institute of Solid State Physics, The University of Tokyo.

[1]G. S. Painter and D. E. Ellis, Phys. Rev. **1**, 4747 (1970).
[2]F. Bassani and G. P. Parravicini, Nuovo Cimento B **50**, 95 (1967).
[3]M. Posternak, A. Baldereschi, A. J. Freeman, E. Wimmer, and M. Weinert, Phys. Rev. Lett. **50**, 761 (1983).
[4]K. I. Bolotin, K. J. Sikes, Z. Jiang, M. Klima, G. Fudenberg, J. Hone, P. Kim, and H. L. Stormer, Solid State Commun. **146**, 351 (2008).
[5]J. B. Oostinga, H. B. Heersche, X. Liu, A. F. Morpurgo, and L. M. K. Vandersypen, Nat. Mater. **7**, 151 (2008).
[6]Y. Zhang, T. Tang, C. Girit, Z. Hao, M. C. Martin, A. Zettl, M. F. Crommie, Y. R. Shen, and F. Wang, Nature **459**, 820 (2009).
[7]M. F. Craciun, S. Russo, M. Yamamoto, J. B. Oostinga, A. F. Morpurgo, and S. Tarucha, Nat. Nanotechnol. **4**, 383 (2009).
[8]S. Y. Zhou, G.-H. Gweon, A. V. Fedorov, P. N. First, W. A. de Heer, D.-H. Lee, F. Guinea, A. H. C. Neto, and A. Lanzara, Nat. Mater. **6**, 770 (2007).
[9]A. Mattausch and O. Pankratov, Phys. Rev. Lett. **99**, 076802 (2007).
[10]N. T. Cuong, M. Otani, and S. Okada, Phys. Rev. Lett. **106**, 106801 (2011).
[11]K. Kamiya, N. Umezawa, and S. Okada, Phys. Rev. B **83**, 153413 (2011).
[12]Y. Takagi and S. Okada, Jpn. J. Appl. Phys., Part 1 **51**, 085102 (2012).
[13]M. Igami, S. Okada, and K. Nakada, Synth. Met. **121**, 1233 (2001).
[14]P. Giannozzi, R. Car, and G. Scoles, J. Chem. Phys. **118**, 1003 (2003).
[15]N. T. Cuong, M. Otani, and S. Okada, Appl. Phys. Lett. **101**, 233106 (2012).
[16]T. O. Wehling, K. S. Novoselov, S. V. Morozov, E. E. Vdovin, M. I. Katsnelson, A. K. Geim, and A. I. Lichtenstein, Nano Lett. **8**, 173 (2008).
[17]Y. H. Zhang, Y. B. Chen, K. G. Zhou, C. H. Liu, J. Zeng, H. L. Zhang, and Y. Peng, Nanotechnology **20**, 185504 (2009).
[18]F. Schedin, A. K. Geim, S. V. Morozov, E. W. Hill, P. Blake, M. I. Katsnelson, and K. S. Novoselov, Nat. Mater. **6**, 652 (2007).
[19]M. Matsubara and S. Okada, Appl. Phys. Express **10**, 025101 (2017).
[20]M. Matsubara and S. Okada, Jpn. J. Appl. Phys., Part 1 **56**, 125101 (2017).
[21]O. Leenaerts, B. Partoens, and F. M. Peeters, Phys. Rev. B **77**, 125416 (2008).
[22]Y. Ma, P. O. Lehtinen, A. S. Foster, and R. M. Nieminen, New J. Phys. **6**, 68 (2004).
[23]H. Amara, S. Latil, V. Meunier, Ph. Lambin, and J.-C. Charlier, Phys. Rev. B **76**, 115423 (2007).
[24]M. M. Ugeda, I. Brihuega, F. Hiebel, P. Mallent, J.-Y. Veuillen, J. M. G. Rodriguez, and F. Yndurain, Phys. Rev. B **85**, 121402(R) (2012).
[25]K. Kishimoto and S. Okada, Appl. Phys. Lett. **110**, 011601 (2017).
[26]M. Matsubara and S. Okada, Jpn. J. Appl. Phys., Part 1 **56**, 075101 (2017).
[27]M. Otani and S. Okada, J. Phys. Soc. Jpn. **79**, 073701 (2010).
[28]K. K. Paulla and A. A. Farajian, J. Phys. Chem. C **117**, 12815–12825 (2013).
[29]Y. A. Saucier, S. Okada, and M. Maruyama, Appl. Phys. Express **10**, 095101 (2017).
[30]P. Hohenberg and W. Kohn, Phys. Rev. **136**, B864 (1964).
[31]W. Kohn and L. J. Sham, Phys. Rev. **140**, A1133 (1965).
[32]Y. Morikawa, K. Iwata, and K. Terakura, Appl. Surf. Sci. **169-170**, 11 (2001).
[33]J. P. Perdew, K. Burke, and M. Ernzerhof, Phys. Rev. Lett. **77**, 3865 (1996).
[34]K. Lee, E. D. Murray, L. Kong, B. I. Lundqvist, and D. C. Langreth, Phys. Rev. B **82**, 081101(R) (2010).
[35]V. R. Cooper, Phys. Rev. B **81**, 161104(R) (2010).
[36]I. Hamada and M. Otani, Phys. Rev. B **82**, 153412 (2010).
[37]D. Vanderbilt, Phys. Rev. B **41**, 7892 (1990).
[38]M. Otani and O. Sugino, Phys. Rev. B **73**, 115407 (2006).
[39]T. Hussain, T. Kaewmaraya, S. Chakraborty, and R. Ahuja, J. Phys. Chem. C **120**, 25256–25262 (2016).
[40]G. S. Rao, T. Hussain, M. S. Islam, M. Sagynbaeva, D. Gupta, P. Panigrahi, and R. Ahuja, Nanotechnology **27**, 015502 (2016).